STUDY ON RESIDUAL STRESS, STRAIN & GRAIN SIZE OF USED MEDICAL IMPLANT & NEW MEDICAL IMPLANTS, COMBINING XRD AND WILLIAM-HALL METHOD

[1]Manjunath.B.Bandi, [2]Dr. B.M.Rajprakash

Department of Mechanical Engineering,
[1]Univesity of Visweswaraya Collage of Engineering, Bengaluru, India.

Abstract : This study has been undertaken to investigate the Residual stress distribution in a used 316L SS medical implant and used 316L SS medical implant. This study also briefly describes the theory and methods of residual stress measurement techniques. Residual stresses are determined from the X-ray diffraction data. The diffraction angle 2θ & FWHM (β_{tot}) is calculated from Gaussian peak for all the peaks obtained, and then the lattice spacing, strain is calculated by plotting the graph between Sinθ(rad) vs β_{tot}* Cosθ, we obtain the strain component from the slope (Cε) and the size component from the intercept (Kλ/*L*). Such a plot is known as a Williamson-Hall plot. Determine the composition of samples by EDAX experiment and calculate the young's modulus. From Hooks low and strain component from the slope (Cε), calculate the residual stress.

Index Terms **– Residual stresses, Gaussian peak, Size component, Strain component.**

I. INTRODUCTION

The simplest definition of residual stresses is as follows: stresses that are locked in a material after it has been deformed and all external forces have been removed [01]. More specifically, the deformation must be non-uniform across the material cross-section in order to give rise to residual stresses. The deformation can result not only from forming operations but also from thermal, chemical processes. Phase transformations during heat treatment also induces sufficient strain to result in plastic deformation, thereby giving rise to residual stresses.

The importance of the effects of residual stress on the fatigue and fracture strength of the processed components of many machine parts and structural components has been recognized alongside that of material deteriorations by heat and force ingestion by processing methods. Consequently, many experimental studies on fatigue crack propagation behaviors or fracture strength and some analytical works for welded joints have been carried out. References [02] and [03] list major summaries on those works. However, studies relating stress analysis and experimental results seem to be few, since the variation of residual stress or redistribution due to a crack extension are considered to make the problem complicated.

During machining, residual stresses within the component due to quenching can redistribute and cause a physical distortion of the component. The resulting failure of the finished component as the dimensional tolerances become altered. In severe cases, dimensional instability (buckling) can occur. This is particularly the case where intricate shapes are produced, such as drive arms and webs. For this reason, it is desirable

In addition to the manufacturing issues, residual stresses may potentially influence the fatigue performance and subsequent service life of the finished component [01, 02].

Manufacturers seek to predict and minimize this instability, but the understanding of microstructures in forged components and the design of manufacturing sequences have traditionally been reliant upon iterative workshop trials and the experience of forging metallurgists. The industry is increasingly recognizing the benefits of computer simulation and there is a drive to implement Finite Element Analysis (FEA) techniques to predict the properties of the final component from the processing parameters, such that integrated optimization of the entire process route can be performed. [05]

Most of the available techniques for the measurement of residual stresses in such thick components, such as x-ray diffraction or hole-drilling are limited to the measurement of surface or near-surface (<1 mm) stresses. Even neutron diffraction, which derives its penetrating power from the weak interaction of neutrons with the matter, has usually been limited to depths of ~25 mm. However, new instruments such as SMARTS at Los Alamos and ENGIN-X at ISIS have been built in the last few years specifically for stress measurement, and these are capable of measuring stresses at greater depths [06].

In this paper, I have discussed varies residual stresses measuring methods comparing the measuring technologies used.

II. TYPES OF RESIDUAL STRESS MEASUREMENT TECHNIQUES.

The materials scientist and the engineer can now access a large number of residual stress measurement techniques. Some are destructive, while others can be used without significantly altering the component; some have excellent spatial resolution, whereas others are restricted to near-surface stresses or to specific classes of material [06]. Here the techniques most commonly used for the characterization of residual stress are reviewed.

These methods rely on the monitoring of changes in component distortion, either during the generation of the residual stresses, or afterwards, by deliberately removing material to allow the stresses to relax [07]

A. Hole drilling method

The undisturbed regions of a sample containing residual stresses will relax into a different shape when the locality is machined, thereby providing data for the back-calculation of residual stress. The machining operation usually involves drilling a hole around which the strain is measured using either a rosette of strain gauges; more interferometry; laser interferometry based on a rosette of indentations or holography. In general terms.

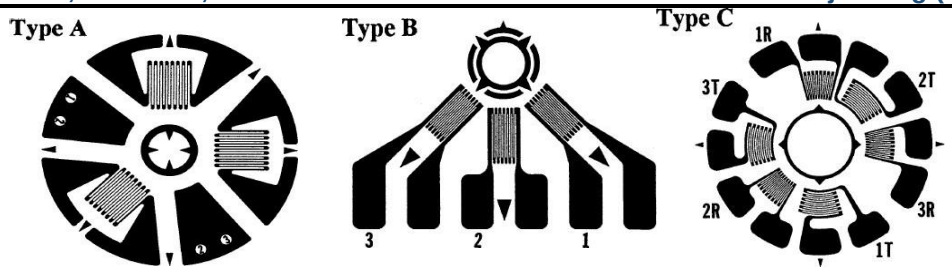

Fig.1: Different types of rosette[8]

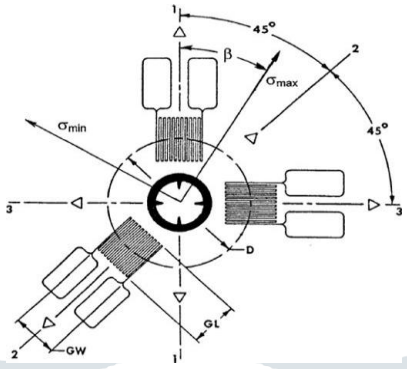

Fig.2: Rosette

$$\varepsilon_r = (\bar{A} + \bar{B}\cos 2\beta)\sigma_{max} + ((\bar{A} - \bar{B}\cos 2\beta)\sigma_{min}$$

The center of the drilled hole shall coincide with the center of the strain gage circle to within either ±0.004 D or ± 0.001in. (±0.025mm), it is recommended that an optical device be used for centering the tool holder.

B. X-ray diffraction method

The typical interatomic spacing in a crystal is of the order of Å, the wavelength of X-ray is of the same order. Since X-ray wavelength and crystal size ae same this results in crystals to act as a diffraction grating for X-radiation

Diffraction = Reflection + Interference (Interference is Constructive or Destructive)

A beam of X-rays directed at crystals, as this ray interacts with the electrons of the atoms in the crystal, it undergoes diffraction and gives rise to intensity distribution with respect to 2theta in the diffracted output, which is characteristic of the crystal structure. The output is known as a diffraction pattern. Diffraction pattern consists of a set of peaks with certain height (intensity) and spaced at certain intervals (X-ray diffraction pattern of a BCC material graph: intensity VS 2theta) X-Ray diffraction has a spatial resolution of 1-2 mm down to tens of μm and a penetration depth of around 10 -30 μ, depending on the material and source.[12]

Limitations of XRD:

1. Geometry of Component
2. Size of Component,
3. Surface roughness of Component, face roughness of Component

C. Synchrotron

Presently, synchrotron diffraction is only available at central facilities, in much the same way as with neutron diffraction.

Two such facilities are

1. European Synchrotron Research Facility in Grenoble,
2. SRS in Daresbury.

Synchrotron = Circular particle accelerator

In synchrotron, charged particles are accelerated to very high speeds, the radiation is known as synchrotron radiation. This radiated energy is very high and using this high intense radiation we get the structure information of crystals and atoms up to very high penetration depth. Advantages of synchrotron radiation is high penetration depth and intense narrow beam. Measurement is very quicker than conventional x-ray diffraction

D. Neutron diffraction

The principle used in neutron diffraction is the same as that of the X-ray Diffraction technique. In neutron diffraction, the 'lattice' stress present in a sample is obtained from the measured elastic 'lattice' strain produced in the crystallites of which it is composed. The lattice strain is determined using Bragg's law of diffraction.

There are essentially two neutron diffraction techniques, namely, conventional h/2h scanning and time of flight approaches. These two methods have developed largely because of the two forms in which neutron beams are available, i.e. as a continuous beam from a reactor source or as a pulsed beam from a spallation source. The former is well suited to conventional h/2h scanning, whereby shifts Dh in a single hkl diffraction peak are monitored according to the equation, while the latter is well In this case, the diffraction profile is not collected as a function of the Bragg angle h, rather the Bragg angle is held constant (usually 2h~90‡) and the incident This is because within each pulse of neutrons leaving the moderated target there is a large range of neutron energies. Naturally, the most energetic neutrons arrive at the specimen first, the least energetic last. Consequently, the energy and hence wave-length of each detected neutron can be deduced from the time that has elapsed since the pulse of neutrons was produced at the target, i.e. In this case, the strain is given by e~Dt/t, where t is the time of flight[37]. As the strain resolution is dependent upon the accuracy of the measurement of the time of flight, high resolution instruments tend to have large flight paths (w100 m).

The choice between the two neutron diffraction methods can be regarded as a choice between measuring all the diffracting neutrons using a single wavelength with the h/2h scan, and measuring the diffracting neutrons for all wavelengths for a fraction of the time with the time of flight approach. In general,

continuous sources tend to offer the best performance when a small region of the whole diffraction profile is required (e.g. single peak based measurements of the macro stress), while time of flight instruments are especially good in situations where a number of peaks, or the whole diffraction profile, is required (e.g. for multiphase materials or where large intergranular strains are to be expected) [15]. At a time of flight instrument, it is most common to use a Riveted refinement to derive a single value of the lattice spacing by simultaneously fitting a curve to the intensity profile from all the reflections within the time of flight capabilities of the instrument. This value is weighted towards those peaks which are most intense and has been shown both experimentally and theoretically to be a very good representation of the bulk elastic response, relatively insensitive to the tensile and compressive shifts of the various reflections.[16]

Results can be obtained with the continuous monochromatic or pulsed polychromatic beam of neutrons. If the spacing of planes change than the strain in the direction of scattering vector Q is given by

$$Q=2\Pi/d$$

$$2d\sin\Theta = n\lambda$$

E. Magnetic method

Magnetostriction & Magnetoelastic effect Magnetic domain aligns with crystalline direction Reduction in magnetoelastic energy calibration of magnetic parameters

Advantages: rapid, portable, biaxial stresses

Limitation: limited material

AWG 31 wire wound around U core to generate 1T Flux density. The signal given to the coil is generated by a waveform generator and amplified by bipolar supply. The generated MBN signal is received by a magnetic read head. The read head probe was mounted permanently inside the ferrite U-core magnet. This read head is coupled with abrupt flux changes within the sample. The signal from the read head is amplified by a preamplifier with a gain of 500, then sent through a bandpass filter (3-200 kHz) Finally, the signal was interfaced with a personal computer that had a resident digital oscilloscope board (Computer scope). The MBN records were stored for subsequent retrieval and analysis

F. Ultrasonic technique

This technique utilizes the result Changes within the speed of supersonic waves during a material are directly laid low with the magnitude and direction of stresses gift within the element.

1. The main activity unit with the inherent chip
2. A group of 2 gauges for the activity of the velocities of supersonic waves thorough the investigated material
3. Supersonic electrical device holder
4. Transportable scope (optional) for the mental image of the supersonic signals
5. Notebook computer (optional) with sophisticated information and a knowledgeable System for analysis of the influence of residual stresses on the fatigue life of welded components

The supporting software package permits dominant the activity method, storing the measured and different information and conniving and plotting the distribution of residual stresses. [12]

G. Raman Technique

The Raman Effect involves the interaction of light with matter. Incident laser light causes the vibration of bonds between atoms. Analysis of the scattered light, known as Raman spectrum, reveals vital information about a sample's physical state and chemical structure. Raman or fluorescence lines shift linearly with variations in hydrostatic stress. This method has fine spatial resolution and by using optical microscopy it is possible to select regions of interest just a few microns in size. The method is essentially a surface strain measurement technique, but with optically transparent materials such as epoxy and sapphire it is even possible to obtain sub-surface measurement. Materials that give Raman spectra include silicon carbide and alumina-zirconia ceramics and the method is particularly useful for studying fiber composites

	Hole Drilling method	**X-Ray Diffraction Method**	**Synchrotron**	**Neutron Diffraction**	**Magnetic Method**	**Ultrasonic Method**	**Raman Method**
Contact or Non contact	-	Non-contact	non-contact	non-contact	Non-contact	contact	Non-contact
Destructive ?	semi-destructive	no	non-destructive	non-destructive	Non-destructive	Non-destructive	Non-destructive
Lab based or portable ?	both	both	lab based method	lab based method	Both	Both	Both
Availability of equipment	Easily available	Generally available	specialist	specialist	generally available	generally available	generally available
Speed	Fast/Med	Fast/Med	fast	Med/ Slow	rapid	rapid	Fast
Standard available	ASTM E-837	No	no	no	No	No	No
Cost of equipment	Low	Med	Government facility	Government facility	Med	Med	Med

Level of expertise require	Low/Med	Med		High	Low	Med	Med
Material Type	Metal/ ceramics /plastics	Metal/ ceramics	Metal/ ceramics	Metal/ ceramics	Ferromagnetic materials	Metal ceramics	polymers ceramics
Composites	yes	yes	yes	yes	No	yes	yes
Crystalline or Amorphous ?	Either	Crystalline	Crystalline	Crystalline	Crystalline	Crystalline	either
Coated ?	yes	yes	yes	no	no	yes	yes
Surface preparation	Important	Important	Important	Not critical	Not critical	Not critical	Not critical
Resolution	50-100µm depth increment	20µm depth 1mm laterally	20µm lateral to incident beam.	500µm	1mm	5 mm	0.5 µm
Penetration	0.4D D= dia of strain gauge circle	5µm-Ti , 50µm-Al , 1mm-layer removal	>500µm 100 mm for Al	100 mm for Al 25 mm for Fe 4 mm for Ti	20-300µm (Barkhausen)	>100 mm Along specimen	Surface

III. RESIDUAL STRESS IN MEDICAL IMPLANT

Statistical evaluations on the concrete number of implant fractures have not been reported in the literature so far. However, national registry data for hip and knee arthroplasty are available that differentiate between fractures occurring in per prosthetic bone and those of the implant material, e.g. the stem of a cement less end prostheses. Even though the data does not always explicitly indicate which component is affected, the total number of revisions due to metallic failure is less than 1%. The overall survival rates of implant systems for trauma, dental or spine surgery are not available. Although the total number of failed implants of one system may be small, implant fracture always has an economic effect: restricted use of such a system up to the system's recall from the market followed by legal consequences and an adverse impact in terms of image for the manufacturer.

Most frequently, failure takes place as a result of high tensile stresses at the surface or around notches, e.g. drill holes in intramedullary nails or plates. Exceeding the critical stress within the thin (1.8–17 nm) 316L stainless steel surface layer may lead to small, superficial micro cracks followed by a fast re passivation. This effect takes place continuously and may even be promoted by the corrosive environment (oxidative wear). In that context, it is known that physiological loading induces unexpected, high cyclic maximum stresses during daily activities. This should be far below the material's critical strength, but may become relevant after a high total number of cycles over its lifetime (high cycle fatigue, HCF). Even the micro cracks within the material, which grow at slow per-cycle velocities (about 10^{-10} to 10^{-9} m/cycle), can propagate to failure throughout course of the implant's lifetime.

From a practical point of view and so that the increased demands of patients can be addressed, implant manufacturers must ask themselves what they can do to increase the fatigue strength of their components. This applies, in particular, to those that have a sophisticated design based on their function:

a) Patient: The external load on the implant may be decreased, e.g. by using crutches, which has a direct impact on the patient's quality of life and is clearly not a permanent solution.
b) Design: The implant's design may be altered to avoid high stress peaks within the material, e.g. by reducing sharp edges. This approach is particularly important when using titanium or titanium alloys as a notch sensitive material, but it is also limited by the available space and the implant's function.
c) Material: According to the field of application, new high-strength materials may be applied, e.g. high-alloyed steels such as CoCrMo. However, they must not only withstand high stresses but also must be appropriate in terms of biocompatibility. In many cases, such as cement less arthroplasty, titanium and its alloys are the only standard material with suitable clinical long-term results. This is certainly the reference material for further developments

IV. LITERATURE REVIEW CONCLUSION

The purpose of this review is to provide an overview of some of the recent advances in the area of residual stress measurement.

- The aim of this literature review is to briefly review residual stress (RS) profiles for 316L SS that are recommended in the main standards, and to identify any new experimental data containing measured or predicted RS profiles.
- There were still limited experimental data on residual stresses measuring system for heterogeneous sample. Only one reference was found which provided measured residual stresses in 316L SS sheet.
- None of the data contained in the literature significantly contradicts the idealized Residual stress profiles provided in the main standards.
- Residual stresses are unavoidably generated in components after welding. The magnitude of residual stresses may be up to the yield strength of the material. Tensile residual stress in engineering structures generally has an adverse effect on structural integrity. It can cause detrimental effects on brittle fracture, corrosion properties and fatigue performance.
- Measurement of residual stresses by the sectioning method has been used for decades to measure residual stresses in Homogeneous sample. This method has proven itself adequate, accurate and economical if proper care is taken in the

preparation of the specimen and the procedure of measurement. However, a standard procedure to carry out to measure residual stresses in heterogeneous sample does not exist in the published literature.

V. OBJECTIVE AND METHODOLOGY

5.1 young's modulus

Experimentally measure composition of metal elements in used 316L SS medical implant and new 316L SS medical implant to determine their young's modulus.

5.2 Residual stresses

Experimentally measure residual stresses.

Measurement of Residua stress is done by XRD method. Here the diffraction angle, 2θ, is measured experimentally and then the lattice spacing is calculated from the diffraction angle, and the known x-ray wavelength using Bragg's Law.

Residual stresses are determined from the diffraction data by calculating the strain from the diffraction peak positions. Any stress, including applied or residual stresses

5.3 William-Hall Plot

Predict residual stress distributions using William-Hall Plot and validate the predictions using the experimental results obtained. we see that by plotting $\beta_{tot}\cos\theta$ versus $\sin\theta$ we obtain the strain component from the slope ($\mathbf{C}\varepsilon$) and the size component from the intercept ($\mathbf{K}\lambda/L$). Such a plot is known as a Williamson-Hall plot.

5.4 Calculation of actual Residual stress.

Determine their young's modulus to calculate the residual stresses with Hook's low

5.5 Results Based on the results assess the impact of the results on medical usage of the implant.

VI. EXPERIMENT AND CALCULATION

The material investigated in this dissertation work is 316L SS O implants Table 5.1 gives the abbreviations of the samples used in the experiment.

Abbreviation	Process
S01	Right part of used sample
S02	Middle part of used sample
S03	Left part of used sample
S04	Right part of New sample 01
S05	Left part of New sample 01
S06	Right part of New sample 02
S07	Left part of New sample 02

1Table 5: The abbreviations of the samples.

6.1 Experiment and calculation of young's modulus

Table 6.1.1, 6.1.2, &6.1.3give chemical composition and Young's modulus of Used 316L SS O implants & new 316L SS O implants

Element Line	Weight %	Weight % Error	Young's modulus GPA	young's modulus of % weight
C K	1.41	± 0.15	27.6	0.38916
Al K	1.72	± 0.37	69	1.1868
Cr K	36.63	± 3.73	279	102.1977
Cr L	---	---		
Fe K	---	---		
Fe L	60.24	± 5.22	210	126.504
Total	100.00			254.58396
Young's modulus	**254.58396GPA**			

Table 6.1.1: Chemical composition and young's modulus of used implant

Element Line	Weight %	Weight % Error	Young's modulus GPA	young's modulus of % weight
C K	1.15	± 0.54	27.6	0.37536
Cr K	36.74	± 20.09	279	102.0246
	62.11	± 8.09	210	130.431
Total	100			**233.3106**
Young's modulus	**233.3106GPA**			

Table 6.1.2: Chemical composition and young's modulus of new implant 01

Element Line	Weight %	Weight % Error	Young's modulus GPA	young's modulus of % weight
O K	2.59	± 0.70		
C K	1.36	± 0.14	27.6	0.37536
Al K	8.54	± 0.67	69	5.9064
Cr K	30.49	± 3.15	279	85.0671
Cr L	---	---		
Fe K	---	---		

Fe L	57.01	± 4.27	210	119.72
Total	100.00			**178.16346**
Young's modulus	**178.16346GPA**			

6.2 Residual Stresses

XRD reading for S01, Right part of used sample

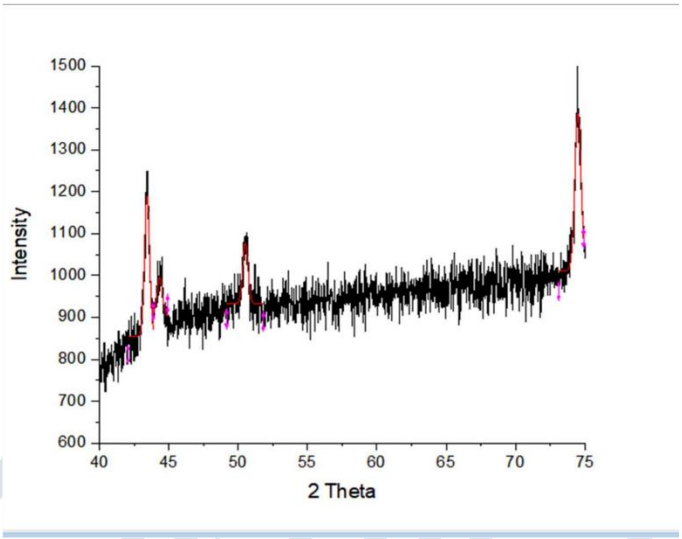

. Graph 5.2.1: x-ray diffraction results for S01.

The data in red indicates smoothening of data with Gaussian equation for calculation of FWHM value. We assume that Increasing in grain boundary length is only due to residual stress developed during the course of time. Other factors influencing increasing in length of grain boundary are

1. Temperature
2. Impact load
3. Chemical treatment
4. Fatigue

The data in red indicates smoothening of data with Gaussian equation for calculation of FWHM value.
Graph 5.2b shows typical x-ray diffraction results of S01, smoothening of data with Gaussian equation for FWHM value

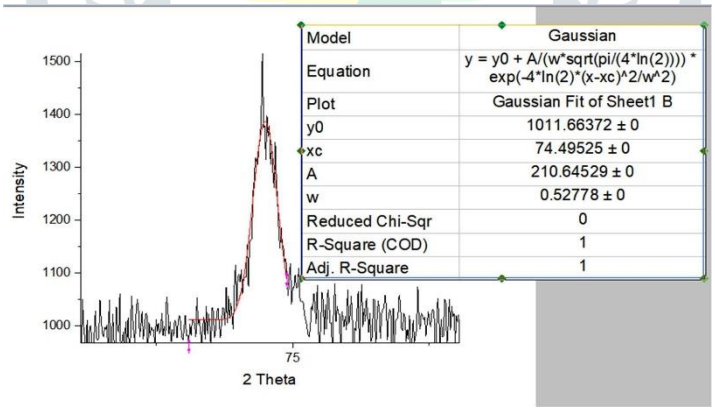

1Graph 5.2.1b shows typical x-ray diffraction results of S01

The function for the intensity at any value of 2θ near the peak becomes:

$$I(2\theta) = Imax\ exp\ [-\pi\ (2\theta - 2\theta 0)2\ /\ \beta 2\ ]$$ Equation 1

where I_{max} is the peak intensity, $2\theta_0$ is the 2θ position of the peak maximum, and the integral breadth, β, is related to the FWHM peak width, H, by

$$\beta = 0.5\ H\ (\pi\ /\ \log_e 2)^{1/2}$$ Equation 2

From the table 5.2.1, 2 θ And FWHM values of all the peaks are used to calculate SinΘ(rad) , FWHM(red) & CosΘ(rad) are given below

2 Θ	Θ (rad)	FWHM(Degree)	FWHM(rad)	Sin Θ (red)	FWHM(rad)* CosΘ (rad)
44.3538	0.38722	0.45064	0.00787	0.37761	0.00729
50.52271	0.44107	0.44459	0.00776	0.42691	0.00702

74.49252	0.65033	0.52778	0.00922	0.60545	0.00733

2Table 6.2.1 SinΘ(rad) , FWHM(red) & CosΘ(rad) of Sample S01

$$B_L = \frac{K\lambda}{L\,Cos\theta}$$

$$\beta e = C\varepsilon\, tan\theta \qquad \text{Equation 3}$$

One contribution varies as 1/cosθ and the other as tanθ. If both contributions are present then their combined effect should be determined by convolution. The simplification of Williamson and Hall is to assume the convolution is either a simple sum or sum of squares (see previous discussion on Sources of Peak Broadening within this section). Using the former of these then we get:

$$\beta\, tot = \beta e + \beta L = C\varepsilon\, tan\theta + \frac{K\lambda}{L\, cos\theta} \qquad \text{Equation4}$$

If we multiply this equation by cosθ we get:

$$\beta tot\, cos\theta = C\varepsilon\, sin\theta + \frac{K\lambda}{L} \qquad \text{Equation 5}$$

And comparing this to the standard equation for a straight line (m = slope; c = intercept)

$$y = mx + c \qquad \text{Equation 6}$$

We see that by plotting $\beta_{tot}\cos\theta$ vs sinθ we obtain the strain component from the slope (Cε) and the size component from the intercept (Kλ/L). Such a plot is known as a Williamson-Hall plot and is illustrated schematically below (All the calculations are done with the help of Origin 8 software)

From the above data plot is drawn between Sin Θ v/s FWHM cos θ

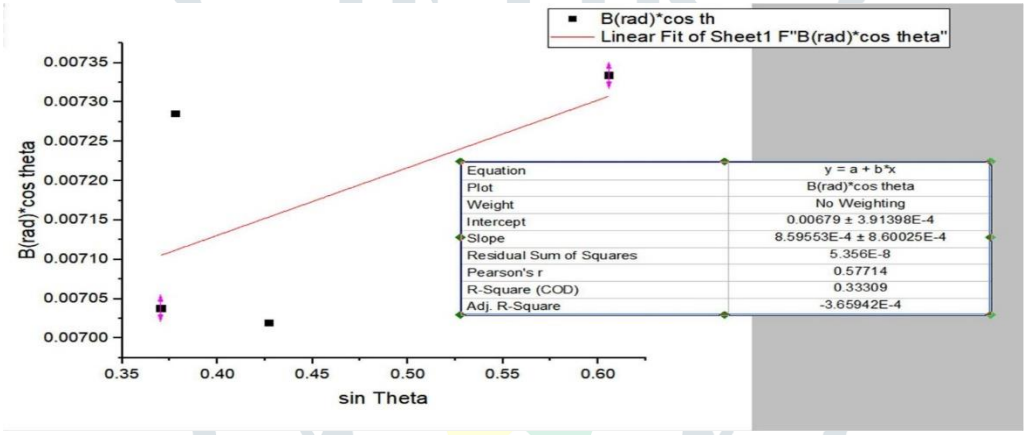

Graph 6.2.1: W H Plot of S01. we see that by plotting $\beta_{tot}\cos\theta$ versus sinθ we obtain the strain component from the slope (Cε) and the size component from the intercept (Kλ/L).

Graph 6.2.1: A linear graph of $\beta_{tot}\cos\theta$ versus sinθ fitted to diffraction data with a Positive slope
Graph 6.2.1: shows a linear fit of data obtained from the x-ray diffraction.
Graph 6.2.1: exhibits a regular $\beta_{tot}\cos\theta$ vs sinθ behavior, which suggests the use of the Equation 16
From graph 6.2
Cε=8.59553E-4 and Intercept = 0.00679

$$\beta tot\, cos\theta = C\varepsilon\, sin\theta + \frac{K\lambda}{L} \qquad \text{Equation 7}$$

$\beta tot \cos 0.488933 = C\varepsilon \sin 0.488933 + \frac{K\lambda}{L}$

$\beta tot = 6.7969 * 10^{-3}$

$$\varepsilon = \frac{\beta tot}{4\tan\theta} \qquad \text{Equation 8}$$

$\varepsilon = \frac{6.7969*10-3}{4\tan 0.488933}$ $\varepsilon = 0.209$

$\sigma = \varepsilon\gamma$

$\sigma = 0.209 * 254.58369$

$\boldsymbol{\sigma = 53.36\ Gpa}$

XRD reading for S02 Right part of used sample
Graph 5.2.2 shows typical x-ray diffraction results for S01.

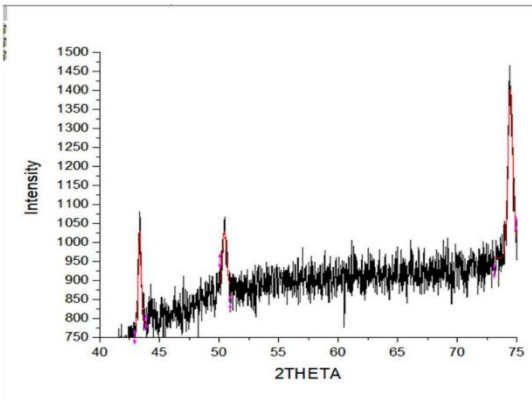

Model	Gaussian
Equation	y = y0 + A/(w*sqrt(pi/(4*ln(2))))
Plot	Intensity
y0	958.6028 ± 6.3
xc	74.4544 ± 0.00
A	237.33383 ± 9.
w	0.50235 ± 0.01
Reduced	1520.64449
R-Square	0.94399
Adj. R-Sq	0.94192

2Graph 5.2.2: x-ray diffraction results for S02.

The function for the intensity at any value of 2θ near the peak becomes:

$$I(2\theta) = Imax\ exp\ [-\pi\ (2\theta - 2\theta o)2\ /\ \beta 2\ ] \qquad \text{Equation 9}$$

where I_{max} is the peak intensity, $2\theta_0$ is the 2θ position of the peak maximum, and the integral breadth, β, is related to the FWHM peak width, H, by

$$\beta = 0.5\ H\ (\pi\ /\ \log_e 2)^{1/2} \qquad \text{Equation 10}$$

From the table 5.2.2, 2 θ And FWHM values of all the peaks are used to calculate SinΘ(rad), FWHM(red) & CosΘ(rad) are given below

2 Θ	Θ (rad)	FWHM(Degree)	FWHM(rad)	Sin Θ (red)	FWHM(rad)* CosΘ (rad)
43.36473	0.75716	0.28439	0.00497	0.68686	0.00461
50.4646	0.88113	0.99241	0.01733	0.77146	0.01461
74.4545	1.3	0.50235	0.00877	0.96356	0.00698

3Table 6.2.2 SinΘ(rad) , FWHM(red) & CosΘ(rad) of Sample S02

From the above data plot is drawn between Sin Θ v/s FWHM cos θ

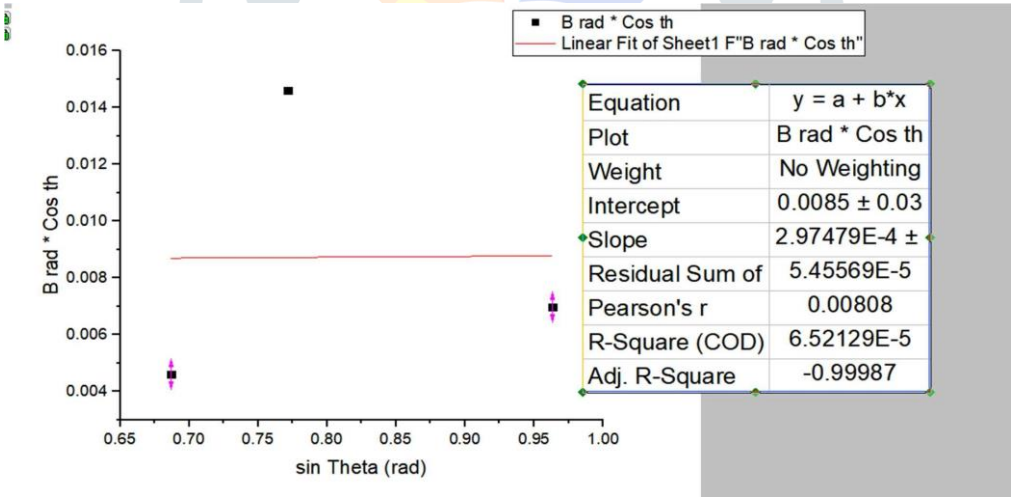

3Graph 6.2.2: W H Plot of S012. we see that by plotting $\beta_{tot}\cos\theta$ versus $\sin\theta$ we obtain the strain component from the slope (Cε) and the size component from the intercept (Kλ/L).

Graph 6.2.2: A linear graph of $\beta_{tot}\cos\theta$ versus $\sin\theta$ fitted to diffraction data with a Positive slope

Graph 6.2.2: shows a linear fit of data obtained from the x-ray diffraction.

Graph 6.2.2: exhibits a regular $\beta_{tot}\cos\theta$ vs $\sin\theta$ behaviour, which suggests the use of the Equation 16

From graph 6.2

Cε=2.97479E-4 And Intercept = 0.0085

$$\beta tot\ cos\theta = C\varepsilon\ sin\theta + \frac{K\lambda}{L} \qquad \text{Equation 11}$$

$$\beta\text{tot}\cos 0.97343 = C\varepsilon \sin 0.97343 + \frac{K\lambda}{L}$$

$$\beta\text{tot} = 10.357 * 10^{-3}$$

$$\varepsilon = \frac{\beta\text{tot}}{4\tan\theta} \qquad \text{Equation 12}$$

$$\varepsilon = \frac{10.357*10-3}{4\tan 0.97343} \qquad \varepsilon = 1.587$$

$\sigma = \varepsilon\gamma$
σ = 1.587*254.58369
$\boldsymbol{\sigma}$ **= 404.24109** $\boldsymbol{Gpa}$

Similarly for S03, S04, S05, S06, &S07 Samples

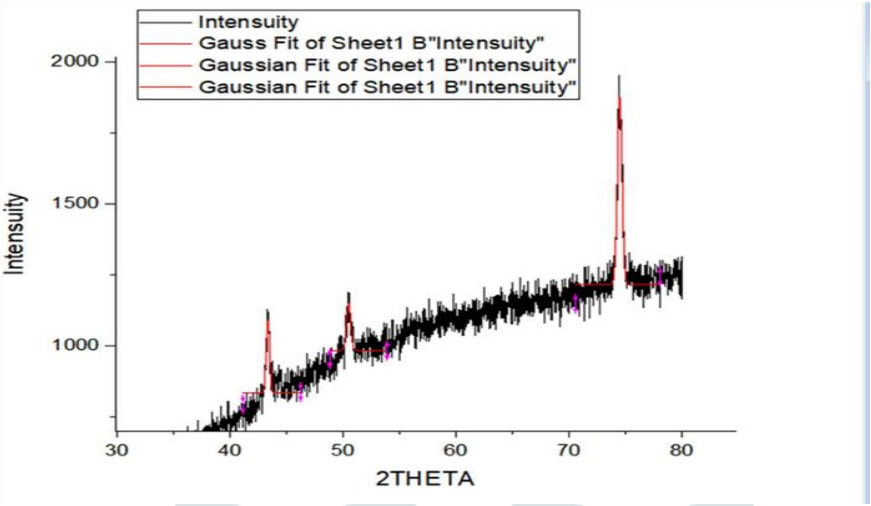

4Graph 5.2.3**:** x-ray diffraction results for S03.

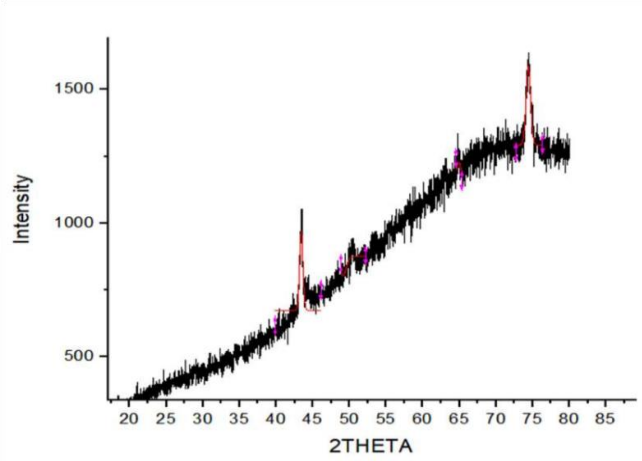

5Graph 5.2.4**:** x-ray diffraction results for S04

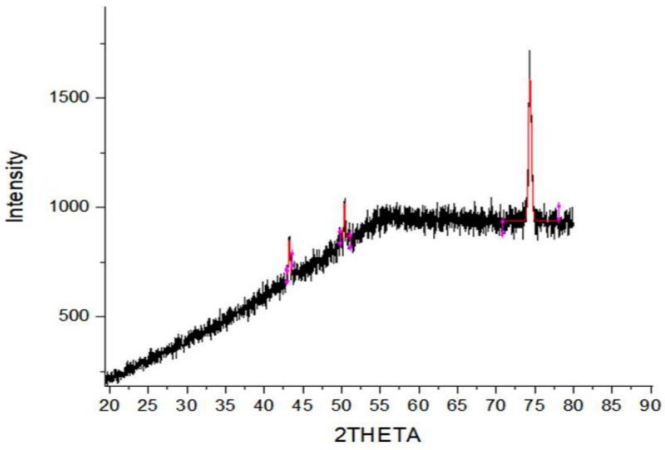

6Graph 5.2.5: x-ray diffraction results for S05

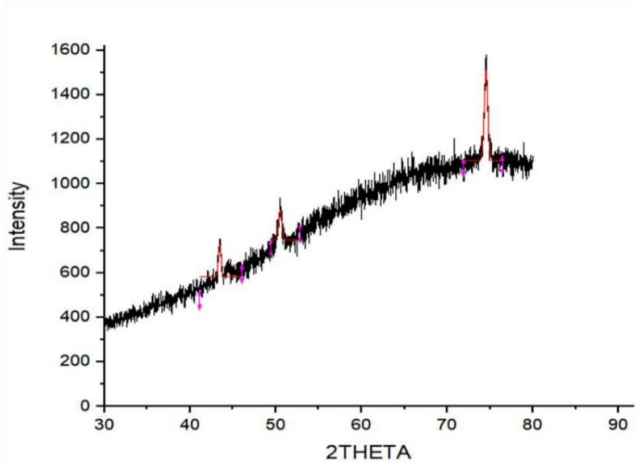

7Graph 5.2.6**:** x-ray diffraction results for S06

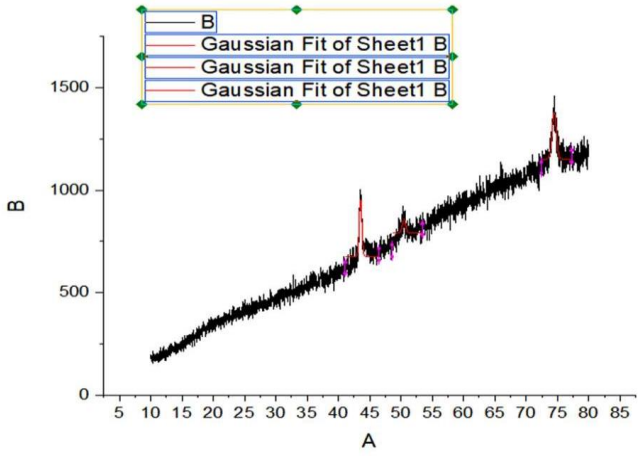

8Graph 5.2.7: x-ray diffraction results for S07.

The residual stress calculation for S03 to S07 is similar to that of S01 & S02. It follows, using equation 16
Hence W-H Plot, data of W-H plot and Residual stresses of remaining samples are listed below

		S03 Middle part of used sample			
2 Θ	**Θ(rad)**	**FWHM (Degree)**	**FWHM(rad)**	**Sin Θ(red)**	**FWHM(rad)* Cos Θ (red)**

43.36856	0.37861	0.32781	0.00572	0.36963	0.00532
50.50247	0.44089	0.45961	0.00802	0.42675	0.00726
74.45924	0.65004	0.48101	0.0084	0.60522	0.00669
		S04 Right part of New sample 01			
2 Θ	**Θ(rad)**	**(Degree)**	**FWHM FWHM(rad)**	**Sin Θ(red)**	**FWHM(rad)* Cos Θ (red)**
43.43488	0.37919	0.54984	0.0096	0.37017	0.00892
64.9032	0.56662	0.5104	0.00891	0.53678	0.00752
74.41402	0.64965	0.74999	0.0131	0.6049	0.01043
		S05 Left part of New sample 01			
2 Θ	**Θ(rad)**	**(Degree)**	**FWHM FWHM(rad)**	**Sin Θ(red)**	**FWHM(rad)* Cos Θ (red)**
43.53786	0.38009	0.50209	0.00877	0.37101	0.00814
50.50298	0.4409	0.6149	0.01074	0.42675	0.00971
74.9586	0.6544	0.80952	0.01413	0.60868	0.01121
		S06 Right part of New sample 02			
2 Θ	**Θ(rad)**	**(Degree)**	**FWHM FWHM(rad)**	**Sin Θ(red)**	**FWHM(rad)* Cos Θ (red)**
43.45608	0.37938	0.37454	0.00654	0.37034	0.00607
50.498	0.44086	0.49582	0.00866	0.42671	0.00783
74.5275	0.65064	0.4797	0.00838	0.60569	0.00666
		S07 Left part of New sample 02			
2 Θ	**Θ(rad)**	**(Degree)**	**FWHM FWHM(rad)**	**Sin Θ(red)**	**FWHM(rad)* Cos Θ (red)**
43.25145	0.37759	0.2165	0.00378	0.36868	0.00351
50.37721	0.4398	0.23546	0.00411	0.42576	0.00372
74.38731	0.64941	0.45396	0.00793	0.60472	0.00631

4Table 6.2.3 SinΘ(rad) , FWHM(red) & CosΘ(rad) of Sample S03 to S07

From the above data plot is drawn between Sin Θ v/s FWHM cos θ

From the Table 6.2.3 data plot is drawn between Sin Theta v/s FWHM cos theta

9Graph 6.2.3: W H Plot of S03 to S07. We see that by plotting $\beta_{tot}\cos\theta$ versus $\sin\theta$ we obtain the strain component from the slope ($C\varepsilon$) and the size component from the intercept ($K\lambda/L$).

Graph 6.2.3: A linear graph of $\beta_{tot}\cos\theta$ versus $\sin\theta$ fitted to diffraction data with a Positive and slopes

Graph 6.2.3: shows a linear fit of data obtained from the x-ray diffraction.

Graph 6.2.3: exhibits a regular $\beta_{tot}\cos\theta$ vs $\sin\theta$ behaviour, which suggests the use of the Equation 16

From graph 6.2.3 Intercept and slope for S03 to S07 are as fallows

	S03	**S04**	**S05**	**S06**	**S07**
Intercept	0.00471	0.00712	0.00417	0.00671	-0.00131
Slope	0.00366	0.00365	0.01176	3.16344E-4	0.01249

5Table 6.2.4 Intercept and slope for S03 to S07

From the data of Table 6.2.2& Table 6.2.3 Residual stress are calculated and listed below

Abbreviation	**Location**	**Residual stresses in GPA**
S01	Right part of used sample	53.36 GPA
S02	**Middle part of used sample**	**404.241093 GPA**
S03	Left part of used sample	54.94399 GPA
S04	Right part of New sample 01	49.05421 GPA

S05	Left part of New sample 01	31.67 GPA
S06	Right part of New sample 02	19.6123 GPA
S07	Left part of New sample 02	-8.21 GPA

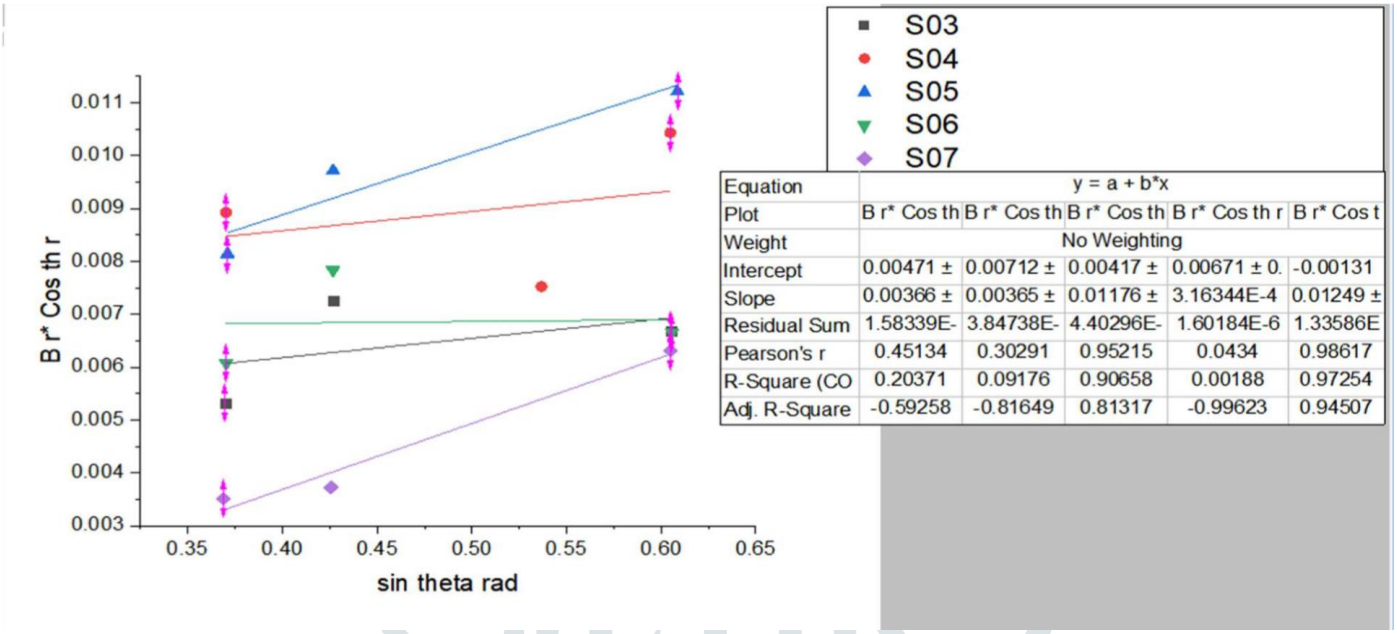

Equation	y = a + b*x				
Plot	B r* Cos th	B r* Cos th	B r* Cos th	B r* Cos th r	B r* Cos t
Weight	No Weighting				
Intercept	0.00471 ±	0.00712 ±	0.00417 ±	0.00671 ± 0.	-0.00131
Slope	0.00366 ±	0.00365 ±	0.01176 ±	3.16344E-4	0.01249 ±
Residual Sum	1.58339E-	3.84738E-	4.40296E-	1.60184E-6	1.33586E
Pearson's r	0.45134	0.30291	0.95215	0.0434	0.98617
R-Square (CO	0.20371	0.09176	0.90658	0.00188	0.97254
Adj. R-Square	-0.59258	-0.81649	0.81317	-0.99623	0.94507

6Table 1.6.4: Residual stresses of sample S01 to S07

For the 7 given samples, the assumption of biaxial method made the calculations straightforward. Using the associated equations for the method the residual stress values of the samples were determined.

6.3 Discussion based on results

The X-ray diffraction (XRD) is one of the best methods for measuring the residual stress. XRD method measures the strain as the distance between crystallographic planes (d-spacing). This method can only be used to crystalline, polycrystalline and semi-crystalline materials. When the material is in stretched, the distance between crystallographic planes increases and when the material is in compression, distance between crystallographic planes decreases. Among the samples S07 have negative intercept values in P-H plot, which means the state of residual stress exist in the samples S07 is compressive. On the other hand, for the rest of the samples have positive intercept values in P-H plot, which means the state of residual stress exist in the remaining samples is tensile.

The presence of residual stresses in the material produces widen in the x-ray diffraction peak position that is directly found by plot between 2 theta VS intensity. In Graph 2 to 8 widen in the peak positions can be observed for different samples. It is important to find a diffraction peak for suitable intensity. The peaks should not contain interference from neighboring peaks. So that the diffraction angle 2-theta can be measured experimentally and the distance between crystallographic planes is then calculated using Bragg's law. Among the seven samples S02 the middle part of used implant is having 404.241093 Gpa of residual stresses. which is because of external force applied by the doctors on the implant during the surgery, from the results it is also found that slight increase in residual stresses in used implant, hence it is recommend that not to reuse or consider the used implant as scrap in medical application especially orthopedic implant.

The common problems in using X-ray diffraction technique arise due to the location of diffraction peak. For peak fitting purposes, the high precision is necessary which in turn requires accurate sample alignment and precise methods of diffraction peak location. One of the major disadvantages with XRD is the limitation imposed on the test piece size and geometry. The geometry has to be such that an X-ray can both hit the measurement area and still be diffracted to the detector without hitting any obstructions. However, due to irregular geometry of some of the samples, it was not possible to get clear diffraction data.

The method is valid for isotropic and anisotropic materials. However it is necessary to have homogenous strain distribution within the material. Experimental data for the seven set of samples indicated that $\beta_{tot}\cos\theta$ V/S $\sin\theta$ behavior is linear

6.4. Sources of Errors

In addition to the factors mentioned in the previous section, a number of factors can contribute to the introduction of error in the measurements. These parameters can be summarized as the following:

1) Collection time.
2) Peak location method.
3) Surface curvature.
4) Aperture size.
5) Oscillation.

6.5. Future Work

In addition to the uniaxial method, biaxial method and triaxle method can be used. The results of these two techniques can be compared.

A better fitting program can be used to get peak values, so that the amount of error introduced during calculation can be reduced.

1) Number of data points can be increased to get more accurate results.
2) Surfaces of the samples can be cleaned using proper chemicals to eliminate any possible error due to surface.

3) Samples can be run more than once, so that repeatability of the technique can be shown.
4) Calculation of proportions of macro and micro stresses.
5) X-ray residual stress determination of textured samples.

REFERENCES

1. Robert Sonntag, [1] Jörn Reinders, [1] Jens Gibmeier, [2] and J. Philippe Kretzer [1] ·Fatigue Performance of Medical Ti6Al4V Alloy after Mechanical Surface Treatments PLoS One. 2015; 10(3): e0121963. 2015 Mar 30
2. E. Brinksmeier, Hannover; J. T. Cammett, Cincinnati; W. Konig (l), Aachen; P. Leskovar (2). Ljubljana; J. Peters (l), Leuven; H. K. Tonshoff (l), Hannover
3. Carlos Oldani and Alejandro Dominguez Department of Materials and Technology, Faculty of Exact, Physical and Natural Sciences, Universidad Nacional de Córdoba Argentina
4. Sethi, T. Kaus, and P. Scohor, "The use of angulatedabutments in implant dentistry: five year clinical results of anongoing prospective study," International Journal of Oral and Maxillofacial Implants, vol. 15, no. 6, pp. 801–810, 2000.
5. Akpinar, F. Demirel, L. Parnas, and S. Sahin, "A comparisonof stress and strain distribution characteristics of two differentrigid implant designs for distal-extension fixed prostheses,"Quintessence International, vol. 27, no. 1, pp. 11–17, 1996.
6. W. Anselm Wiskott and U. C. Belser, "Lack of integrationof smooth titanium surfaces: a working hypothesis basedon strains generated in the surrounding bone," Clinical OralImplants Research, vol. 10, no. 6, pp. 429–444, 1999.
7. D. R. Carter, M. C. Van der Meulen, and G. S. Beaupre,"Mechanical factors in bone growth and development," Bone,vol. 18, no. 1, supplement 1, pp. S5–S10, 1996.
   A. Kashi, A. R. Chowdhury, and S. Saha, "Finite element analysisof a TMJ implant," Journal of Dental Research, vol. 89, no. 3, pp.241–245, 2010.
8. H. Van Oosterwyck, J. Duyck, J. Vander Sloten, G. Van DerPerre, and I. Naert, "Periimplant bone tissue strains in casesof dehiscence: a finite element study," Clinical Oral Implants Research, vol. 13, no. 3, pp. 327–333, 2002.
9. S. Faegh and S. Muftu, "Load transfer along the bone-dentalimplant interface," Journal of Biomechanics, vol. 43, no. 9, pp. 1761–1770, 2010.
10. D. H. Detolla, S. Andreana, A. Patra, R. Buhite, and B. Comella,"Role of the finite element model in dental implants," The Journal of Oral Implantology, vol. 26, no. 2, pp. 77– 81, 2000.
11. G. Menicucci, A. Mossolov, M. Mozzati, M. Lorenzetti, andG. Preti, "Tooth-implant connection: some biomechanicalaspects based on finite element analyses," Clinical Oral ImplantsResearch, vol. 13, no. 3, pp. 334–341, 2002.
12. S. Tada, R. Stegaroiu, E. Kitamura, O. Miyakawa, and H.Kusakari, "Influence of implant design and bone qualityon stress/strain distribution in bone around implants: a 3dimensional finite element analysis," International Journal ofOral and Maxillofacial Implants, vol. 18, pp. 357–368, 2003.
13. P. Geng, K. B. Tan, and G. R. Liu, "Application of finite elementanalysis in implant dentistry: a review of the literature," TheJournal of Prosthetic Dentistry, vol. 85, pp. 585– 598, 2001.
14. W. Xu, J. H. Wang, J. Geng, and H. M. Huang, "Application ofcommercial FEA software," in Application of the Finite ElementMethod in Implant Density